Rheol Acta (2002) 41: 461–470
© Springer-Verlag 2002

ORIGINAL CONTRIBUTION

David J. Eyre
Graeme W. Milton
Roderic S. Lakes

Bounds for interpolating complex effective moduli of viscoelastic materials from measured data

Received: 10 August 1999
Accepted: 21 December 2000

D. J. Eyre · G. W. Milton (✉)
Department of Mathematics
University of Utah, Salt Lake City
UT 84112 USA
e-mail: milton@math.utah.edu

R. S. Lakes
Department of Engineering Physics
University of Wisconsin, Madison
WI 53706 USA

Abstract The complex effective moduli of viscoelastic materials can be experimentally measured by a number of techniques giving relaxation data for materials at discrete frequencies. In this paper we present a method which allows one to find bounds on the moduli of the material at the unmeasured frequencies. Our bounds can be very tight, and are, therefore, good approximations to the data. Using our bounds, experimentalists can concentrate their efforts on gathering highly accurate data at only a few frequencies and numerically generate data at other frequencies that may be of interest.

Keywords Viscoelasticity · Complex moduli · Relaxation · Bounds

Introduction

The physical reality of viscoelastic behavior may be represented mathematically by a variety of functions of time or frequency. The complex dynamic function of frequency is regarded as most closely related to direct perception. All these functions are interrelated, see for example Gross (1947, 1953); most of the exact relationships are integral transforms. For example, the transient time dependent functions which describe creep (strain response to step stress) or relaxation (stress response to step strain) are related to the dynamic functions which describe the response to sinusoidal input, by a one-sided sine or cosine Fourier transform. For the complex dynamic moduli, the real and imaginary parts are related by the Kramers-Kronig relations (Kronig 1926; Kronig and Kramers 1928), which are integral transforms.

Frequency-dependent data must be taken at close intervals if there is any possibility of resonance. For example, a structural system may have one or more natural resonant frequencies; see Lakes (1998) and Lee et al. (2000). If the damping is small, the structural compliance exhibits a sharp peak requiring closely spaced measurements to resolve. In measurements of relaxing systems on the continuum scale one does not expect resonance provided the frequency in question is sufficiently below the lowest natural frequency of the microstructure. It is the purpose of this paper to explore the question of the required density of data points to characterize properly relaxing systems, and to elucidate the question of inferences one can make for frequencies higher or lower than those available in the data. The upper frequency limit is dictated by experimental limitations such as resonance in the apparatus. The lower frequency limit is usually dictated by the patience of the experimenter.

At all but the highest frequencies, the response of many linear viscoelastic materials can be well approximated by a relaxation model, which neglects microinertial effects in the stress-strain relation for the material itself, possibly a composite. The macroscopic force-displacement relation for a structural element will exhibit structural resonance even in the absence of micro-resonance. For example, consider a complex relaxation modulus $G^*(p) = G'(p) + iG''(p) = |G^*(p)|e^{i\delta(p)}$ as a function of $p = i\omega$ for an isotropic viscoelastic material, where ω is the frequency.

In this paper, we will only treat the case of measurements of G^* at real values of ω, corresponding to values of p along the positive imaginary axis.

However measurements at complex values of ω, obtained through free damped vibration experiments (Struik 1967), could also be easily incorporated into the bounds. The underlying theory remains valid: only measurements at purely imaginary values of ω, corresponding to positive real values of p, need special attention.

In accordance with linear viscoelastic theory, the relaxation model says this function has the integral representation (see Schwarzl and Struik 1967; Ferry 1972)

$$G^*(p) = G_e + \int_0^\infty \frac{H(\tau)d\tau}{1 + 1/(p\tau)}, \tag{1}$$

where $G_e = G^*(0)$ is real and non-negative (zero if the material has Newtonian flow) and $H(\tau)$ is a positive real-valued distribution function of relaxation times τ. Here τ is called the relaxation time. If the distribution of relaxation times is discrete (i.e., $H(\tau)$ is a sum of delta functions) then $G^*(p)$ is a rational function of p with its poles and zeros alternating along the negative real p axis, with a zero nearest or at the origin and a pole nearest infinity, and with the poles having negative residues.

The function $G^*(p)$ is analytic in the entire complex plane with possible exceptions on the negative real p-axis. Additionally, the function is positive and real on the positive real p-axis, has positive imaginary part for $p'' > 0$, and finally, $G^*(p) = \overline{G^*(\bar{p})}$, where the bar denotes complex conjugation. Therefore, knowing the value of G^* (p_j) also gives the value of $G^*(\bar{p}_j)$, but such known values will not be incorporated (except in the derivation of the bounds) since the information they contain is redundant with the integral representation for $G^*(p)$.

Often experimental data for $G^*(p)$ are analyzed by making some additional assumptions about $H(\tau)$. Commonly used models include fitting the data to a delta function spectrum or to a box function spectrum. In the latter case, the box spectrum function (Tobolsky 1960) is taken to be

$$H(\tau) = \begin{cases} H_0 & \text{if } \tau_1 \le \tau \le \tau_2 \\ 0 & \text{otherwise} \end{cases} \tag{2}$$

and then the data is used to try to fit the positive parameters τ_1, τ_2, and H_0. Such spectra have been used in the modeling of polymer materials in superposition with other spectra to achieve sufficient flexibility to reproduce accurately experimental data (see Lakes and Katz 1979; Tobolsky 1960). Box spectra are mathematically convenient because they generate simple test models for which the functions $G^*(p)$ can be explicitly calculated.

Rather than making these ad-hoc assumptions about the form of $H(\tau)$, this paper provides bounds, for any frequency ω_0, on $G_0 = G^*(p_0)$ where $p_0 = i\omega_0$. The bounds incorporate measured values $G_j = G^*(p_j)$ of the function $G^*(p)$ at N positive real frequencies, $\omega_1, \omega_2, \ldots, \omega_N$ which correspond to N values $p_1, p_2, \ldots, p_N$ along the positive imaginary axis. We will refer to these values as *anchor points*. Our bounds interpolate these data values and bound $G^*(p)$ at values of p where G^* has not been measured. Moreover, the bounds we provide are the *sharpest possible* within the class of functions compatible with functions that can be represented by the integral given in Eq. (1), and the bounds provide *analytically admissible approximants* to the experimental data.

Specifically this paper addresses the question: given that one knows how a material responds to oscillatory inputs at a set of N frequencies, what bounds can one place on its response at another frequency?

Our analysis is based on the observation that this bounding problem is essentially the same as one which has been solved by one of the authors (Milton 1981). There bounds were derived on the complex effective permittivity ε_e of a composite made from two isotropic phases with complex permittivities ε_1 and ε_2, given values of the function ε_e $(\varepsilon_1, \varepsilon_2)$ at N possibly complex pairs $(\varepsilon_j^1, \varepsilon_j^2)$ (see also McPhedran and Milton 1981, where the bounds were numerically computed and tested). Due to the homogeneity of this function (i.e., due to the fact that $\varepsilon_e(c\varepsilon_1, c\varepsilon_2) = c\varepsilon_e(\varepsilon_1, \varepsilon_2)$ for all real and complex values of c) the problem can be reduced to bounding $\varepsilon_e(p, 1)$ given the value of $\varepsilon_e(p, 1)$ at N possibly complex values $p_j = \varepsilon_j^1/\varepsilon_j^2$, and additionally the value $\varepsilon_e(1, 1) = 1$. [This is also closely tied to the problem of bounding Stieltjes functions, since the function $f(z) = [\varepsilon_e(1+z, 1)–1]/z$ is a Stieltjes function of z with a radius of convergence around $z = 0$ of at least 1 (see, for example, Milton 1986) satisfying the additional constraint that $f(-1) \le 1$. Common (1968) and Baker (1969) derive bounds on Stieltjes functions $f(z)$ having a known radius of convergence and known values of $f(z)$ at N points. However they assumed that the known values were for N real values of z and so their bounds are not appropriate to the present problem.]

The derivation in Milton (1981) was based on the analytic properties of $\varepsilon_e(p, 1)$, which were rigorously established by Golden and Papanicolaou (1983). These analytic properties are the same as those of the function $G^*(p)$ of interest here: in particular, the function $\varepsilon_e(p, 1)$ has an integral representation directly analogous to Eq. (1). The only difference is that now the value of $G^*(1)$ is not known. As shown in the Appendix, the proof of the bounds is easily adapted to the present case where one does not know the value of $G^*(1)$. The bounds we derive apply to arbitrary functions $G^*(p)$ satisfying Eq. (1): no assumptions are made beyond the non-negativity of G_e and $H(\tau)$.

The bounds confine G_0 to lie inside a lens shaped region in the complex plane for any given value of p_0. The lens shaped region moves and varies in size as p_0 is

varied and collapses to a point when $p_0 = p_1, p_2, \ldots$ or p_N. The region is described as the intersection of two circles that are given by rational functions of p_0 (having a discrete relaxation spectrum) that are compatible with the data and which have one free parameter. Determining each of these two circles in the complex plane involves varying the free parameters while interpolating the known data values. In this paper, we describe the rational functions that define the bounds, and give examples of their use to bound data.

One cautionary remark: before applying the bounds it is necessary to check that the measured values G_1, G_2,..., G_N at the anchor points are themselves compatible with the integral representation at Eq. (1). This is ensured provided the imaginary part of G_N is positive and that G_k, for $k = N–1, N–2, \ldots, 1$, lies inside the lens shaped region associated with the bounds incorporating the $N–k$ known values $G_{k+1}, G_{k+2}, \ldots, G_N$.

The remainder of this paper is divided into three sections. In the next section, the bounds are used to bound and approximate the moduli of materials that have box relaxation spectra and used to bound and approximate experimental relaxation data for an alloy made from cadmium and magnesium. In the following section, we describe the bounds and their calculation, and we give a brief justification of them. Finally, we describe how the bounds can be used by experimentalists to obtain data at unmeasured frequencies. In the Appendix we provide the proof of the bounds.

Examples of the use of the bounds

The practical utility of our bounds will be demonstrated with two sets of examples. In the first set of examples, the bounds are applied to model problems with box relaxation spectra. In the second set of examples, the bounds are applied to experimentally obtained data describing the relaxation of cadmium-magnesium alloys.

The bounds applied to model spectra

If the relaxation spectra are a sum of delta functions, the material moduli corresponding to these types of spectra are rational functions (Gross 1953). Our bounds are themselves rational and they interpolate the data provided. Therefore, if the number of data points that are being interpolated is sufficiently large, our bounds will exactly recover the complex moduli of these materials.

Our bounds are applied to model problems with box relaxation spectra in Figs. 1 and 2. For real values of the frequency ω_0 the material moduli $G_0 = G^*(i\omega_0) = G'_0 + iG''_0$ corresponding to the spectrum given by Eq. (2) are

$$G'_0 = \frac{H_0}{2}\log\left(\frac{1+\omega^2\tau_2^2}{1+\omega^2\tau_1^2}\right) \tag{3}$$

and

$$G''_0 = H_0\left[\tan^{-1}(\tau_2\omega) - \tan^{-1}(\tau_1\omega)\right] \ , \tag{4}$$

where we have assumed that $G_e = 0$. When our bounds are applied to a box whose support is small, i.e., box spectrum that approximates a delta spectrum, the resulting bounds are very tight because our bounds can exactly recover the delta function. Even when the support of the box is large, the bounds are reasonably tight as seen in Fig. 1. Here we take $H_0 = 1$, $\tau_1 = 0.01$, and $\tau_2 = 100$. We use two points to anchor our bounds, at $p_1 = 0.01i$ and $p_2 = 100i$ and show the bounds for both the real and imaginary parts of $G_0 = G^*(p_0) = G'_0 + iG''_0$.

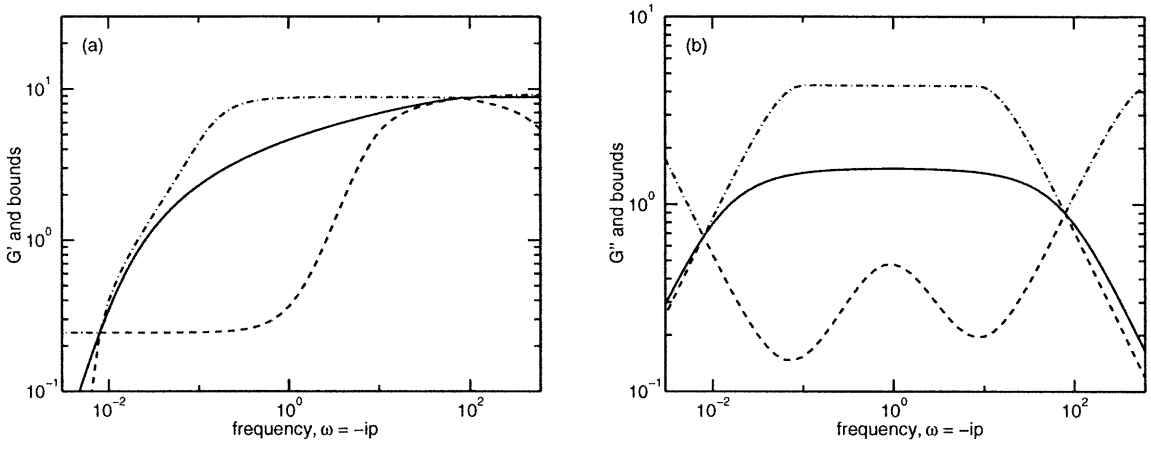

Fig. 1a, b Real and imaginary parts of the material moduli with its upper and lower bounds where the materials distribution function is defined by a box spectrum. These bounds were generated using only two data points

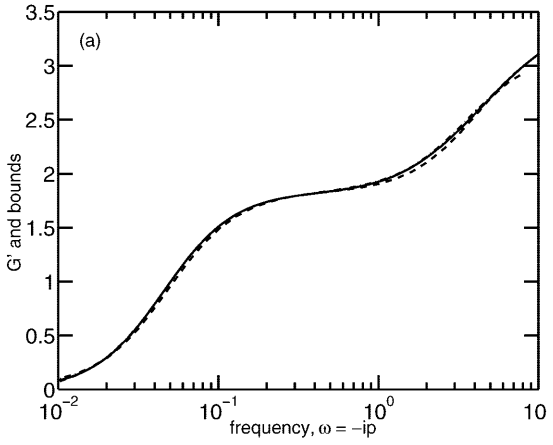

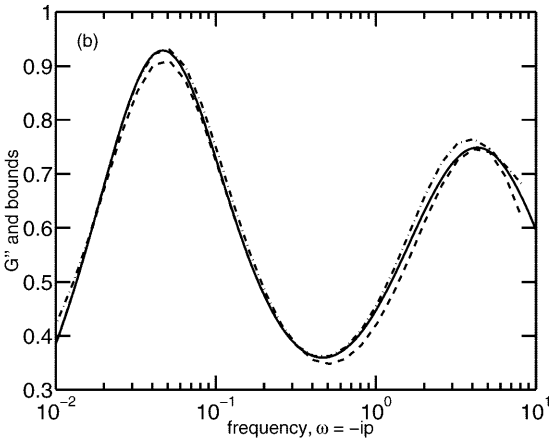

Fig. 2a, b Real and imaginary parts of the material moduli with its upper and lower bounds where the materials distribution function is defined by two box spectra. These bounds were generated using three data points. We have found similar results when the anchors are chosen closer together as well

In all of this paper's figures, the anchors are easy to find since they are the points where the bounds interpolate the data.

In Fig. 2, we take a spectrum composed of two disjoint boxes. The first box has $H_0 = 1$, $\tau_1 = 0.1$, and $\tau_2 = 0.5$ and the second box has $H_0 = 10$, $\tau_1 = 20$, and $\tau_2 = 24$. The sum of the spectrum with these two boxes are qualitatively different than the single boxes. Three anchor points, at $p_1 = 0.02i$ and $p_2 = 0.3i$, $p_3 = 5i$, for our bounds are used. The bounds are tight again, and with only two anchors, the bounds capture the apparent inflection points in $G_0' = G'(p_0)$ and the two maxima and the minimum of $G_0'' = G''(p_0)$.

The bounds in Fig. 2 are much tighter than the bounds in Fig. 1 because the range of the data in Fig. 2 is an order of magnitude smaller, the box spectra have smaller support, and the bounds in Fig. 2 incorporate three anchor points whereas the bounds in Fig. 1 incorporate only two anchor points.

The bounds applied to cadmium-magnesium data

In this section, the bounds are applied to experimentally obtained viscoelastic properties of cadmium-magnesium alloys. The alloy used and the experiments performed to obtain these data are described in Cook and Lakes (1995). In Figs. 3, 4, and 5, we take two, three, and four anchor points, respectively, and we show how incorporating more information by including more anchors can tighten the bounds.

In Fig. 3, experimentally obtained data and a set of two point bounds are shown. The bounds are displayed as solid lines. These bounds were generated by using the experimental data with anchors taken at 0.1 and 56.23 Hz. No other information from the experimental data was used to generate these bounds. Figure 3a Shows the bounds for $\tan\delta_0 = G_0''/G_0'$ and Fig. 3b shows the

Fig. 3a, b Data and two point $\tan\delta_0$ and $|G_0|$ bounds for cadmium-magnesium alloys without errors (*solid lines*) and with errors (*dashed lines*). The anchors are taken at 0.1 Hz and 56.23 Hz: **a** the bounds for $\tan\delta_0$; **b** the bounds for $|G_0|$

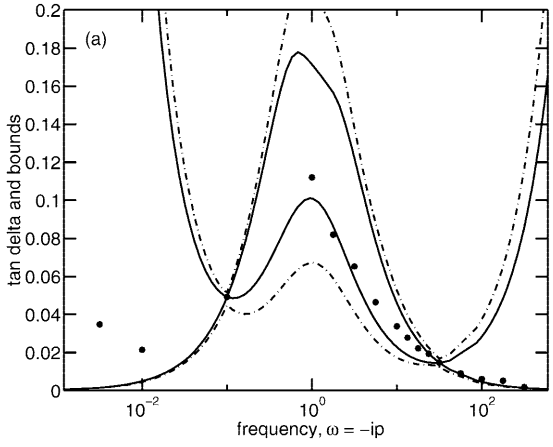

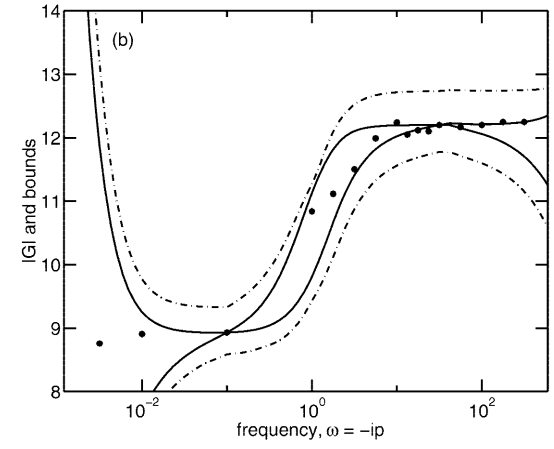

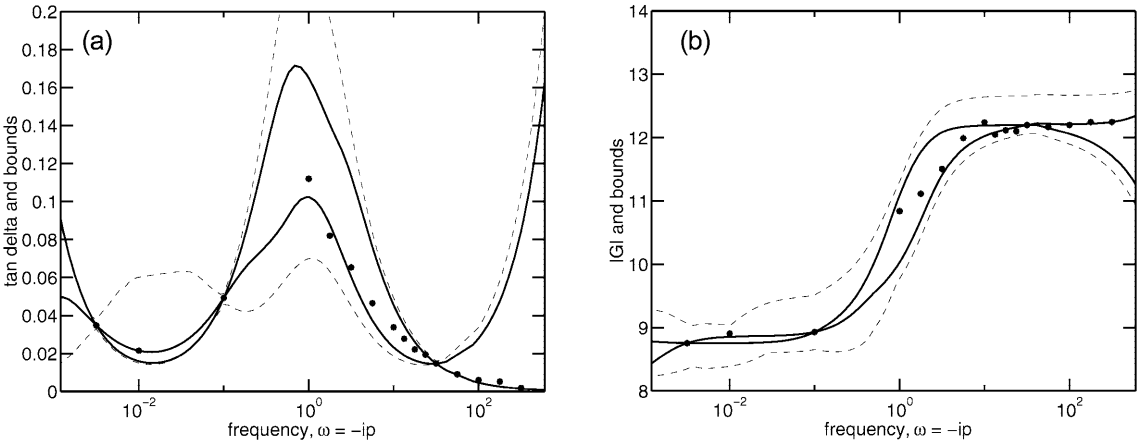

Fig. 4a, b Data and three point $\tan\delta_0$ and $|G_0|$ bounds for cadmium-magnesium alloys without errors (*solid lines*) and with errors (*dashed lines*). The anchors are taken at 0.00320, 0.1, and 56.23 Hz: **a** the bounds for $\tan\delta_0$; **b** the bounds for $|G_0|$

bounds for $|G_0|$. Notice that all but one of the measurements of $\tan\delta_0$ are consistent with the bounds, and all but three measurements of $|G_0|$ are consistent with the bounds, and in each of these cases, the deviation of the data from the bounds is less than the error estimates for the experimental results.

When the data and their errors are outside the bounds, there are two possibilities. First, the measurements at the anchors contain enough error to produce inconsistent bounds or, second, the bounds reflect the fact that the remaining data are not perfect. In the second case if the deviation of the data from the bounds exceeds error estimates, then one would do well to seek sources of error not accounted for initially.

We now address the first case where the anchors contain errors. The dashed curves in Fig. 3 show the bounds when errors have been added to the anchor points in a Monte-Carlo simulation. We generated anchors near the experimental values as

$$G_j^{\text{new}} - G_j^{\text{old}} + \varepsilon_j' + i\varepsilon_j'' \quad \text{for } j = 1, 2, \ldots, \tag{5}$$

where ε_j' and ε_j'' are independently generated from Gaussian distributions with mean zero and variance equal to 5% of the real and imaginary parts of G_j^{old}. We then computed the bounds for 30 realizations, excluding those realizations, if any, where the combination G_1^{new}, G_2^{new},..., G_N^{new} was incompatible with the integral representation at Eq. (1) (i.e., which were such that for some value of k the value of G_k^{new} lay outside the lens shaped region associated with the bounds incorporating the N–k values G_{k+1}^{new}, G_{k+2}^{new},...,G_N^{new}). The dashed curves in Fig. 3a show the maximum upper and minimum lower bounds for $\tan\delta_0$ and in Fig. 3b shows the maximum extent of upper and lower bounds for $|G_0|$ in the presence of these errors.

In Fig. 4, experimentally obtained data and a set of three point bounds are shown. These bounds were generated by using the experimental data with anchors

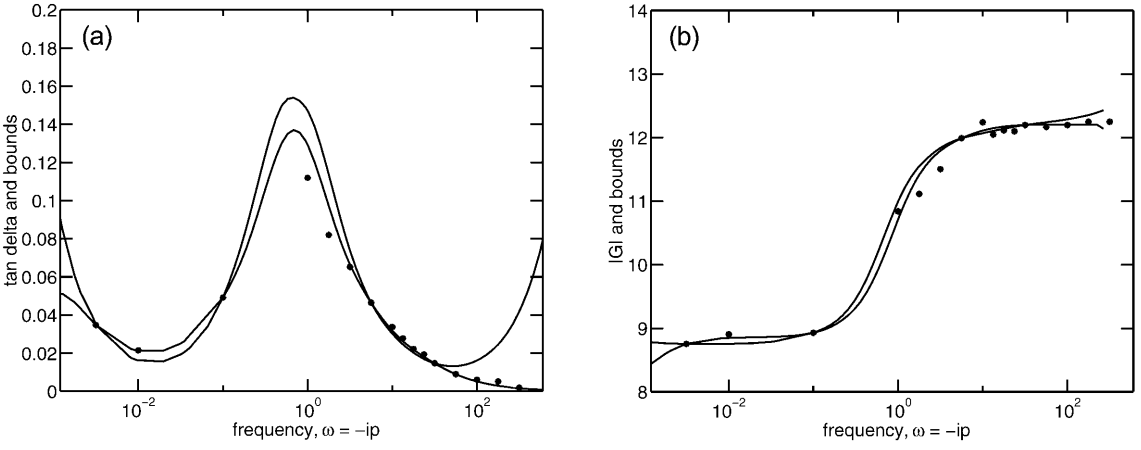

Fig. 5a, b Data and four point $\tan\delta_0$ and $|G_0|$ bounds for cadmium-magnesium alloys. The anchors are taken at 0.01, 0.1, 5.62, and 31.62 Hz: **a** the bounds for $\tan\delta_0$; **b** the bounds for $|G_0|$

taken at 0.00320, 0.1, and 56.23 Hz. Figure 4a shows the bounds for $\tan\delta_0$ and Fig. 4b shows the bounds for $|G_0|$. Notice that by adding the new anchor, the bounds are tightened at lower frequencies.

The dashed curves in Fig. 4 show the bounds when errors have been added to the anchor points in a Monte-Carlo simulation. Again, we generated anchors near the experimental values as described above, but here using Gaussian distributions which with mean zero and variance equal to 3% of the real and imaginary arts of G_j^{old}. We then computed the bounds for 30 realizations. The dashed curves in Fig. 4a show the maximum upper and minimum lower bounds for $\tan\delta_0$ and in Fig. 4b shows the maximum upper and minimum lower bounds for $|G_0|$ in the presence of these errors.

In Fig. 5, experimentally obtained data and a set of three point bounds are shown. These bounds were generated by using the experimental data with anchors taken at 0.00320, 0.01, 13.34, and 56.23 Hz. Figure 5a shows the bounds for $\tan\delta_0$ and Fig. 5b shows the bounds for $|G_0|$. In these bounds, either the accuracy of both $\tan\delta_0$ and $|G_0|$ of several of the data values between 1 and 10 Hz should be questioned or the accuracy of the anchor values should be questioned. If the anchor values are assumed to be correct, then these four point bounds could be used to approximate the data at intermediate frequencies.

In practice, if many anchors are used, the experimental data must be very accurate to find rational functions that interpolate the data and are analytically consistent. While it may be difficult to obtain this data experimentally, the bounds offer the advantage that they are tight for a small number of anchors. Thus one should concentrate on measuring a small number of values with high accuracy.

Finally, we do not know of a method other than by computation of measuring the change in the bounds when the data is subject to experimental error. However, the Monte-Carlo procedure used above could be readily performed on any data set and gives an idea of how sensitive the bounds are to errors in the anchor points being used.

A description of the bounds

To describe the bounds, suppose that $G^*(p)$ has been measured at N frequencies on the positive imaginary p-axis (i.e., positive real ω). The real and imaginary parts of $G^*(p)$ at these points provide $2N$ constraints on our bounds.

The bounds are the simplest possible rational functions which interpolate the $2N$ constraints, and which are consistent with the integral representation of the complex moduli given in Eq. (1). The rational functions that satisfy these requirements are one of the following two possibilities:

- The first rational function interpolates the data, and has N simple poles and N simple zeros interlaced along the negative real axis with a zero closest to the origin and a pole closest to infinity. The position of the poles and zeros and the amplitude of the candidate function, a total of $2N+1$ parameters, are partially determined by the $2N$ known constraints leaving one parameter free. As this parameter is varied, while keeping the frequency fixed, the value of the rational function inscribes a circle in the complex plane. This circle is one of two defining the bounds in the complex plane at the given frequency.

- The second rational function interpolates the data, has N simple poles and N simple zeros interlaced along the negative real axis, and has one additional zero at $p=0$ and one additional pole at $p=\infty$. Again, the positions of the poles and zeros and the amplitude of the function, a total of $2N+1$ parameters, are partially determined by the $2N$ known constraints leaving one parameter free. This parameter is varied, keeping frequency fixed, to determine the second circle defining the bounds in the complex plane.

The two circles intersect in the complex plane, and their intersection is a lens shaped region for every frequency. At any frequency ω_0, the bounds on the real and imaginary parts of $G_0=|G_0|\exp(i\delta_0)$ are the minimum and maximum of the real and imaginary parts of the lens shaped region for $p_0=i\omega_0$. The bounds on $|G_0|$ and $\tan\delta_0$ are obtained from the maximum and minimum values of these quantities over the boundary of the lens shaped region.

Since the proof of these bounds is technical it is given in the Appendix. It rests on a straightforward extension of the analysis in Milton (1981). Briefly, $G^*(p)$ can be approximated by a rational function of very high degree with its poles and zeros alternating along the negative real axis, and its poles having negative residues. The positions of the poles and zeros of the rational function and its amplitude can then be varied to find the range in the complex plane over which $G_0=G^*(p_0)$ varies while maintaining the known values $G^*(p_j)=G_j$ at the frequencies, p_1, p_2,..., p_N. Because the known values G_j are complex, this provides $2N$ constraints. An examination of first-order variations shows that a necessary condition for G_0 to be at the boundary of its range is that the total number of poles and zeros of $G^*(p)$, not counting any zero at the endpoint $p=0$ and not counting any pole at the endpoint $p=\infty$, must not exceed $2N$. Such rational functions, satisfying the known values,

have one free parameter and fall into two classes according to whether or not the function has a zero at $p=0$. As the free parameter is varied in each class, G_0 inscribes a circular arc in the complex plane. The two arcs generated in this way form the boundary of the lens.

The bounds on G_0' and G_0'' are computed numerically. To do this, we express the numerator and denominator of the bounds as polynomials using a power basis. Let $\mathcal{G}_i(p)$ denote the i-th bound. In the first bound, the degrees of the numerator and denominator are equal, so

$$\mathcal{G}_1(p) = \frac{\sum_{i=0}^{N} a_i p^i}{\sum_{i=0}^{N} b_i p^i} \quad , \tag{6}$$

where the parameters a_i and b_i are real, and $a_N=1$ is our usual normalization. The second bound has a zero at the origin and a pole at infinity, so the degree of the numerator is $N+1$, and

$$\mathcal{G}_2(p) = \frac{p\sum_{i=0}^{N} \alpha_i p^i}{\sum_{i=0}^{N} \beta_i p^i} \quad , \tag{7}$$

where again the parameters α_i and β_i are real, and $\beta_N=1$ is our normalization.

The remaining coefficients of the polynomials are then determined by the constraint that the bounds interpolate the data,

$$\mathcal{G}_i(p_j) = G_j, \text{ for } j = 1, 2, \ldots, N \ . \tag{8}$$

The real and imaginary parts of these constraints provide a set of $2N$ linear equations on these coefficients. This set of equations has $2N+1$ unknowns, and its solutions determine the circle in the complex plane described above. Values on the circle are determined by two steps. First fixing one coefficient and solving for the remaining $2N$ coefficients with the $2N$ equations determines the rational function $\mathcal{G}_i(p)$. The function $\mathcal{G}_i$ evaluated at $p=p_0=i\omega_0$ gives a point on one of the circles at the desired frequency ω_0, and the circle can be traced by choosing all possible real values for the free parameter. Fortunately, this can be simplified.

The center and radius of a circle can be defined by any three points on the circle. With our bounds, two of these three points are easy to determine. Our bounds coincide at the two points where the circles intersect. These points correspond to $a_0=0$ and $b_N=0$ in the first bound and $\alpha_N=0$, and $\beta_0=0$ in the second bound. We will denote the two functions defining the intersection points of the $\mathcal{G}_{12}(p)$ and $\mathcal{G}_{21}(p)$ These functions are found using the first bound to interpolate the anchor points G_i, with the normalization $a_N=1$ and with $a_0=0$ in the first case and with $b_N=0$ in the second case.

One point on each bound must still be determined for every frequency. To find this point on the first bound, we choose the normalization $a_N=1$ and the free parameter to be b_N. For the second bound, we choose the normalization $\beta_N=1$ and the free parameter to be α_N. These choices are convenient because when the free parameter is zero, they reduce to the points where the bounds intersect. To find a reasonable choice for the free parameter, we numerically minimize the condition number of the linear system equations one must solve to find the radius and center of the circle given three points on the circle. We used the Nelder-Mead algorithm for the minimization (see Dennis and Woods 1987) and note that what we seek is a point that allows us to find the circle accurately. Therefore, finding a minimum is unimportant; we only seek a reasonable condition number of the linear system defining the center and radius.

The lens shaped region that defines the bounds is itself bounded by one arc from each of the two circles. The circles consist of two arcs – the arc that defines the lens and the remaining arc. To determine which arc is part of the lens, the third point found above can be used once more. If the distance between that point and the center of the other circle is smaller than the radius of the other circle, then the third point lies on the arc that defines the lens. If the distance is larger than the radius, the other arc of the circle defines the lens.

Given the anchor points for the bounds, they are computed with the following algorithm. For each $p=i\omega$ where the bounds are desired:

- Find the two intersecting points of the two circles using the first bound with $a_0=0$ first and then with $b_N=0$ and evaluating the intersection functions at $p = i\omega$.
- Find a third point on each bound by choosing the free parameter of the bounds to minimize the condition number of the linear system of equations that defines the circles from three points.
- Determine which arc of the circles define the lens shaped bounds.
- Determine the minimum and maximum real and imaginary parts of the lens.

An alternative approach to finding the third point is based on the observation that when p_0 is taken to be real, say $p_0=\omega_t$ where ω_t is chosen to be some typical frequency in the range of interest, the lens shaped region collapses to an interval on the real axis extending between $\mathcal{G}_{12}(\omega_t)$ and $\mathcal{G}_{21}(\omega_t)$ We choose b_N and α_N so that $\mathcal{G}_1(\omega_t)$ and $\mathcal{G}_2(\omega_t)$ equal some intermediate point, which we take to be say the geometric average of the endpoints:

$$\mathcal{G}_1(\omega_t) = \mathcal{G}_2(\omega_t) = \sqrt{\mathcal{G}_{12}(\omega_t)\mathcal{G}_{21}(\omega_t)} \ . \tag{9}$$

With these chosen values of b_N and α_N the arc joining $\mathcal{G}_{12}(p_0)$ and $\mathcal{G}_{21}(p_0)$ which passes through $\mathcal{G}_1(p_0)$ and the

arc joining $\mathscr{G}_{12}(p_0)$ and $\mathscr{G}_{21}(p_0)$ which passes through $\mathscr{G}_2(p_0)$ define the bounds for all complex values of p_0.

Conclusions

As our examples demonstrate, the bounds can be very tight, even when only a few data points are incorporated.

This should allow experimentalists to simplify their method of measurement since they should now need far less data to obtain equal results. Alternatively, an experimentalist could use our bounds in combination with their data to detect when the relaxation model breaks down. Even when the relaxation model breaks down $G'(p)$ and $G''(p)$ should still be compatible with the bounds derived in Milton et al. (1997). Since those bounds are based on weaker assumptions about $G^*(p)$ they are nowhere near as tight as the bounds discussed in this paper when $G^*(p)$ is known to have the integral representation at Eq. (1). Additionally, the bounds derived in Milton et al. (1997) require measurements of the imaginary part of $G^*(p)$ over an entire frequency interval and the real part at a selected number of frequencies while the bounds given here only require measurements of $G^*(p)$ at a discrete set of frequencies.

Our bounds are not as strong when the anchor points are at widely spaced frequencies. In this case, the bounds diverge rapidly at high frequencies above the data and low frequencies below the data. Furthermore, the bounds require more data to become tight enough to use as a reasonable approximation to the data at the unmeasured frequencies.

Acknowledgments The work of GWM and DJE was supported by the General Motors Corporation and the National Science Foundation through grants DMS-0108626, DMS-9803748, DMS-9629692, and DMS-9402763. The work of RSL was supported by the National Science Foundation through grant CMS9896284. The authors are particularly grateful to one of the referees for many valuable comments, and especially for noticing an error in our integral representation for $G^*(p)$, which was subsequently corrected. They also acknowledge the influential role of L.O. Murphy.

Appendix: Proving the bounds

The bounds described in this paper can be established via the method of variation of poles and zeros (Milton 1981). Here we show how this method works in the present context. Our goal is to obtain bounds on $G_0 = G^*(p_0)$ which hold for all rational functions $G^*(p)$ satisfying the required analytic constraints and which have degree m, where m is very large. Since irrational functions in the required class can be approximated arbitrarily closely by rational ones, we can then obtain bounds for irrational functions by taking the limit as m approaches infinity.

Rational functions $G^*(p)$ can be represented as a product:

$$G^*(p) = A\frac{(p-q_1)(p-q_3)\dots(p-q_{2m-1})}{(p-q_2)(p-q_4)\dots(p-q_{2m})} \quad , \tag{A1}$$

in which the q_i are the zeros, for odd i, and poles, for even i, of the function. The analytic properties of the function $G^*(p)$ imply (Schwarzl and Struik 1967) that the amplitude A must be positive and that the poles and zeros are interlaced along the negative real axis, satisfying

$$q_{2m} \le q_1 \le q_{2m-2} \le q_3 \dots \le q_{2m-3} \le q_2 \le q_{2m-1} \le 0 \ , \tag{A2}$$

where the unusual labeling of indices has been chosen to simplify subsequent formulae, as will be explained later.

The quantities $-1/q_i$ are called retardation times, for odd i, and relaxation times, for even i. Since we wish to consider only those functions which interpolate the data, we have the constraints

$$G^*(p_j) = A\frac{(p_j-q_1)(p_j-q_3)\cdots(p_j-q_{2m-1})}{(p_j-q_2)(p_j-q_4)\cdots(p_j-q_{2m})} = G_j, \quad \text{for } j = 1,2,\dots,2N. \tag{A3}$$

where we have chosen to set

$$p_{j+N} = \bar{p}_j,\ G_{j+N} = \bar{G}_j,\ j = 1,2,...,N \tag{A4}$$

in which the bar denotes complex conjugation. The constraint on $G^*(p_{j+N})$ is a corollary of the constraint on $G^*(p_j)$ because the function $G^*(p)$ satisfies $G^*(p) = \overline{G(\bar{p})}$. It is conceivable that the known values G_j may have to be slightly perturbed to ensure that there exist suitable rational functions (rather than only irrational functions) interpolating these known values. We will assume this has been done, although it turns out that there are always suitable rational functions of degree $m = N$ interpolating the known values, whenever there exists an interpolating irrational function.

We will additionally assume that q_{2m} satisfies the constraint that

$$q^- \le q_{2m} \ , \tag{A5}$$

where q^- is very large and negative. (Ultimately we will want to take the limit as q^- approaches minus infinity.) This assumption is convenient because by making it we ensure that the set of points (A, q_1, q_2,..., q_{2m}) where the constraints are satisfied is a closed bounded set. (The amplitude A cannot be zero or take unboundedly large values because then the constraints at Eq. (A3) would be violated.) Consequently, for $p = p_0$, the range of values $G_0 = G^*(p_0)$ takes in the complex plane as (A, q_1, q_2,..., q_{2m}) varies over all admissible values will also be closed and bounded, and consequently any given value on the boundary of the range must be achieved at some (possibly non-unique) point (A', q'_1, q'_2,..., q'_{2m}). Now if the position of a pole happens to coincide with the

position of a zero, we can cancel this common factor from the numerator and denominator in Eq. (A1) and reduce the degree m by 1.

Accordingly, by reducing the value of m as necessary, we can assume that

$$q^- \leq q'_{2m} < q'_1 < q'_{2m-2} < q'_3 \cdots < q'_{2m-3} < q'_2 < q'_{2m-1} \leq 0 \tag{A6}$$

The next step is to explore the effect on $G_0 = G^*(p_0)$ when we perturb the positions of the poles and zeros while still maintaining the $2N$ constraints at Eq. (A3).

We choose $(q_1, q_2, \ldots, q_{2N})$ as our set of $2N$ dependent variables to be determined from the $2N$ equations Eq. A3 and $(A, q_{2N+1}, q_{2N+2}, \ldots, q_{2m})$ as our set of $2(m - N) + 1$ independent variables. (There is some freedom in the choice of independent and dependent variables, but we require that q_{2m} and q_{2m-1} be kept independent to make it easier to keep track of the constraints $q^- \leq q_{2m}$ and $q_{2m-1} \leq 0$. We took an unusual indexing of the poles and zeros to ensure that the constrained pole and constrained zero are last in sequence.) The implicit function theorem implies that Eq. (A3) have a solution for the dependent variables in terms of the independent ones, at least for $(A, q_1, q_2, \ldots, q_{2m})$ in a neighborhood of the point $(A', q'_1, q'_2, \ldots, q'_{2m})$ provided the Jacobian

$$J = \begin{vmatrix} \frac{-G_1}{p_1-q_1} & \frac{G_1}{p_1-q_2} & \frac{-G_1}{p_1-q_3} & \cdots & \frac{G_1}{p_1-q_{2N}} \\ \frac{-G_2}{p_2-q_1} & \frac{G_2}{p_2-q_2} & \frac{-G_2}{p_2-q_3} & \cdots & \frac{G_2}{p_2-q_{2N}} \\ \vdots & \vdots & \vdots & & \vdots \\ \frac{-G_{2N}}{p_{2N}-q_1} & \frac{G_{2N}}{p_{2N}-q_2} & \frac{-G_{2N}}{p_{2N}-q_3} & \cdots & \frac{G_{2N}}{p_{2N}-q_{2N}} \end{vmatrix} \tag{A7}$$

is non-zero when we set $(A, q_1, q_2, \ldots, q_{2m})$ equal to $(A', q'_1, q'_2, \ldots, q'_{2m})$.

Aside from the factors of $G_1, G_2, \ldots, G_{2N}$ and the signs of each column, which are easily factored out, this is one of those special matrices for which an exact formula is available for the determinant (see, for example, Noble 1969) and we have

$$J = \frac{(-1)^N \left[\prod_{n=1}^{2N} G_n\right] \left[\prod_{n=1}^{2N-1} r_n s_n\right]}{\prod_{k=1}^{2N} \prod_{\ell=1}^{2N} (p_k - q_\ell)} \ , \tag{A8}$$

where

$$r_n = \prod_{k=n+1}^{2N} (p_n - p_k), \ s_n = \prod_{k=n+1}^{2N} (q_n - q_k) \ . \tag{A9}$$

From the inequalities at Eq. (A6) it is now clear that the Jacobian as given by Eq. (A7) is non-zero when we set $(A, q_1, q_2, \ldots, q_{2m})$ equal to $(A', q'_1, q'_2, \ldots, q'_{2m})$. Now by differentiating Eqs. (9) and (A2) with respect to the independent variable q_i with $i \geq 2N + 1$, we obtain the set of equations

$$\begin{pmatrix} -1 & \frac{-G_0}{p_0-q_1} & \frac{G_0}{p_0-q_2} & \frac{-G_0}{p_0-q_3} & \cdots & \frac{G_0}{p_0-q_{2N}} \\ 0 & \frac{-G_1}{p_1-q_1} & \frac{G_1}{p_1-q_2} & \frac{-G_1}{p_1-q_3} & \cdots & \frac{G_1}{p_1-q_{2N}} \\ 0 & \frac{-G_2}{p_2-q_1} & \frac{-G_0}{p_2-q_2} & \frac{-G_2}{p_2-q_3} & \cdots & \frac{G_2}{p_2-q_{2N}} \\ \vdots & \vdots & \vdots & \vdots & & \vdots \\ 0 & \frac{-G_{2N}}{p_{2N}-q_1} & \frac{G_{2N}}{p_{2N}-q_2} & \frac{G_{2N}}{p_{2N}-q_3} & \cdots & \frac{G_{2N}}{p_{2N}-q_{2N}} \end{pmatrix} \begin{pmatrix} DG_0/Dq_i \\ Dq_1/Dq_i \\ Dq_2/Dq_i \\ Dq_3/Dq_i \\ \vdots \\ Dq_{2N}/Dq_i \end{pmatrix}$$

$$= (-1)^{i+1} \begin{pmatrix} \frac{G_0}{p_0-q_i} \\ \frac{G_1}{p_1-q_i} \\ \frac{G_2}{p_2-q_i} \\ \vdots \\ \frac{G_{2N}}{p_{2N}-q_i} \end{pmatrix} \ , \tag{A10}$$

where $G_0 = G^*(p_0)$ and D/Dq_i denotes the derivative with respect to q_i at $p = p_0$ while keeping the remaining independent variable fixed, and adjusting the dependent variables so that the constraints at Eq. (A3) remain satisfied. Using Cramer's rule, the solution to these equations for DG_0/Dq_i can be expressed as the ratio of two determinants of the form at Eq. (A7), and with the aid of the formula at Eq. (A8) for such determinants we see that

$$\frac{DG_0}{Dq_i} = \frac{(-1)^i G_0 \left[\prod_{n=1}^{2N} (p_0 - p_n)\right] \left[\prod_{n=1}^{2N} (q_n - q_i)\right]}{(p_0 - q_i) \left[\prod_{n=1}^{2N} (p_n - q_i)\right] \left[\prod_{n=1}^{2N} (p_0 - q_n)\right]} \ . \tag{A11}$$

Similarly, by differentiating Eqs. (A1) and (A3) with respect to the independent variable A, we obtain the set of equations

$$\begin{pmatrix} -1 & \frac{-G_0}{p_0-q_1} & \frac{G_0}{p_0-q_2} & \frac{-G_0}{p_0-q_3} & \cdots & \frac{G_0}{p_0-q_{2N}} \\ 0 & \frac{-G_1}{p_1-q_1} & \frac{G_1}{p_1-q_2} & \frac{-G_1}{p_1-q_3} & \cdots & \frac{G_1}{p_1-q_{2N}} \\ 0 & \frac{-G_2}{p_2-q_1} & \frac{G_2}{p_2-q_2} & \frac{-G_2}{p_2-q_3} & \cdots & \frac{G_2}{p_2-q_{2N}} \\ \vdots & \vdots & \vdots & \vdots & & \vdots \\ 0 & \frac{-G_{2N}}{p_{2N}-q_1} & \frac{G_{2N}}{p_{2N}-q_2} & \frac{-G_{2N}}{p_{2N}-q_3} & \cdots & \frac{G_{2N}}{p_{2N}-q_{2N}} \end{pmatrix} \begin{pmatrix} DG_0/DA \\ Dq_1/DA \\ Dq_2/DA \\ Dq_3/DA \\ \vdots \\ Dq_{2N}/DA \end{pmatrix}$$

$$= - \begin{pmatrix} \frac{G_0}{A} \\ \frac{G_1}{A} \\ \frac{G_2}{A} \\ \vdots \\ \frac{G_{2N}}{A} \end{pmatrix} \ , \tag{A12}$$

where D/DA denotes the derivative with respect to A while keeping the remaining independent variables fixed, and adjusting the dependent variables so that the constraints at Eq. (A3) remain satisfied. Now

observe that, for odd values of i, the right hand side of Eq. (A10) when multiplied by q_i/A reduces to the right hand side of Eq. (A12) in the limit $q_i \to \infty$. It follows that

$$\frac{DG_0}{DA} = \lim_{q_i \to \infty} \frac{q_i}{A}\frac{DG_0}{Dq_i} \text{ for odd } i \ , \tag{A13}$$

and by substituting Eq. (A11) in this formula we have

$$\frac{DG_0}{DA} = \frac{G_0}{A}\frac{\left[\prod_{n=1}^{2N}(p_0 - p_n)\right]}{\left[\prod_{n=1}^{2N}(p_0 - q_n)\right]} \ . \tag{A14}$$

When p_0 is complex we look for points (A', q'_1, q'_2,..., q'_{2m}) such that G_0 is at the boundary of its range of possible values. At such points, the derivatives DG_0/Dq_i and DG_0/Dq_j (where q_i and q_j, with $i \neq j$, are two unconstrained independent variables) if both non-zero must be such that

$$\arg\frac{DG_0}{Dq_i} = \arg\frac{DG_0}{Dq_j} \ , \tag{A15}$$

since otherwise G_0 could be pushed outside the boundary by small variations in q_i and q_j away from q'_i and q'_j. However, at the point (A', q'_1, q'_2,..., q'_{2m}) the four products in Eq. (A11) which are enclosed in square brackets are each either real and non-zero or independent of i and non-zero, and therefore can be factored out. We conclude that the condition at Eq. (A15) can never be satisfied because $\arg(p_0–q'_i) \neq \arg(p_0–q'_j)$ when p_0 is complex and $i \neq j$. This contradiction can only be resolved when at most one unconstrained independent variable q_i, exists. The variable q_j, if independent, must be constrained, i.e., either $j = 2m$, $q'_j = q^-$ and $q_j–q'_j$ is constrained to be positive, or $j = 2m–1$, $q'_j = 0$ and $q_j–q'_j$ is constrained to be negative.

Similarly, the derivatives DG_0/Dq_i and DG_0/DA (where q_i is an unconstrained independent variable) if both non-zero must be such that

$$\arg\frac{DG_0}{Dq_i} = \arg\frac{DG_0}{DA} \ , \tag{A16}$$

and from Eqs. (A11) and (A14) we see that this condition can never be satisfied at the point (A', q'_1,q'_2,..., q'_{2m}) because $\arg(p_0–q'_i) \neq \arg(A') = 0$ when p_0 is complex. Therefore for G_0 to be on the boundary there can only be one unconstrained independent parameter, namely the amplitude A. Either we have $m = N$, or alternatively we have $m = N + 1$ and the variables q'_{2m} and q_{2m} satisfy the constraints $q_{2m-1} = 0$ and $q'_{2m} = q^-$. In the limit as q^- approaches minus infinity, this latter constraint is equivalent to requiring that the bound has a pole at $p = \infty$. This establishes the bounds described in this paper. The key to the proof is the factorization of the derivatives DG_0/Dq_i and DG_0/DA as in Eqs. (A11) and (A14).

References

Baker GA (1969) Best error bounds for Padé approximants to convergent series of Stieltjes. J Math Phys10:814–820

Common AK (1968) Padé approximants and bounds to series of Stieltjes. J Math Phys 9:32–38

Cook LS, Lakes RS (1995) Viscoelastic spectra of $Cd_{0.67}MgO_{0.33}$ in torsion and bending. Met Trans 26A:2037–2039

Dennis JE, Woods DJ (1987) In: Wouk E (ed) New computing environments: microcomputers in large-scale computing. SIAM, Philadelphia

Ferry JD (1972) Viscoelastic properties of polymers, 2nd edn. Wiley, New York

Golden K, Papanicolaou GC (1983) Bounds for effective parameters of heterogeneous media by analytic continuation. Commun Math Phys 90:473–491

Gross B (1947) On creep and relaxation. J Appl Phys 18:212–221

Gross B (1953) Mathematical structure of the theories of viscoelasticity. Actualites Scientifiques et Industrielles 1190 ''Rheologie'', Publications de L'Institut National de Technologie Brésil, Hermann and Cie, Paris

Kronig R (1926) On the theory of dispersion of X-rays. J Opt Soc Am 12:547–555

Kronig R, Kramers HA (1928) Zur Theorie der Absorption und Dispersion in den Röntgenspektren. Z Phys 48:174–179 (in German)

Lakes RS (1998) Viscoelastic solids. CRC Press, Boca Raton, Florida; see also http://silver.neep.wisc.edu/~lakes/FixFree.gif

Lakes RS, Katz JL (1979) Viscoelastic properties of wet cortical bone. III. A non-linear constitutive equation. J Biomech 12:689–698

Lee T, Lakes RS, Lal A (2001) Resonant ultrasound spectroscopy for measurement of mechanical damping: comparison with broadband viscoelastic spectroscopy. Rev Sci Instr 71:2855–2861

McPhedran RC, Milton GW (1981) Bounds and exact theories for the transport properties of inhomogeneous media. Appl Phys A 26:207–220

Milton GW (1981) Bounds on the transport and optical properties of two-component composite materials. J Appl Phys 52:5294–5304

Milton GW (1986) Modeling the properties of composites by laminates. In: Ericksen JL, Kinderlehrer D, Kohn R, Lions J-L (eds) Homogenization and effective moduli of materials and media; the IMA volumes in mathematics and its applications 1. Springer, Berlin Heidelberg New York, pp 150–174

Milton GW, Eyre DJ, Mantese JV (1997) Finite frequency Kramers Kronig relations: bounds on the dispersion. Phys Rev Lett 79:3062–3065

Noble B (1969) Applied linear algebra. Prentice-Hall, NJ, pp 223–224

Schwarzl FR, Struik LCE (1967) Analysis of relaxation measurement. Adv Mol Relaxation Processes 1:201–255

Struik LCE (1967) Free damped vibrations of linear viscoelastic materials. Rheol Acta 6:119–129

Tobolsky AB (1960) Properties and structure of polymers. Wiley, New York